Chapter 4

Rheological measurements with rough walls

4.1 Motivation

The previous experimental work of Koos et al. (2012) provided evidence of the presence of slip at the walls. Such slip can lead to marred conclusions if the rheological measurements are not corrected. The presence of slip can lead to measurements of lower effective relative viscosities, as was shown by Koos et al. (2012). In the case of particles denser than the liquid, the centripetal force due to the rotation of the outer cylinder would tend to push the particles away from the inner cylinder, increasing the depletion layer thickness and thus reducing the measured torques. The slip at the wall can be reduced by roughening the walls of the experiment (Barnes, 1995; Buscall et al., 1993). For this reason, all the experiments presented in this work were conducted with rough walls.

Aside from reducing the slip, rough walls are expected to enhance particle interactions. One of the aims of this work is to study the effect of such interactions on the bulk rheology of the flow.

4.2 Polystyrene particles with matched fluid density

The direct torque measurements for a volume fraction (ϕ) of 10, 20, and 30% as a function of the shear rate ($\dot{\gamma}$) are shown in Figure 4.1. Each point represents the mean of at least five individually recorded measurements; the uncertainties in measuring the torque are combined in root mean square sense (see Section 2.3) and are represented by the error bars. As mentioned in Chapter 2, the torque measurements presented here are directly measured and no correction due to contributions of friction or fluid turbulence is made. The plots also include a linear curve fit for each set of data ($R^2 = 0.993$ for 10%, $R^2 = 0.982$ for 20% and $R^2 = 0.984$). A linear relation between the torque and shear rate would correspond to a Newtonian behavior. However, the linear fit for these measurements does not intercept the origin; instead the linear fit has a negative intercept. As shown in Figure 4.1, the

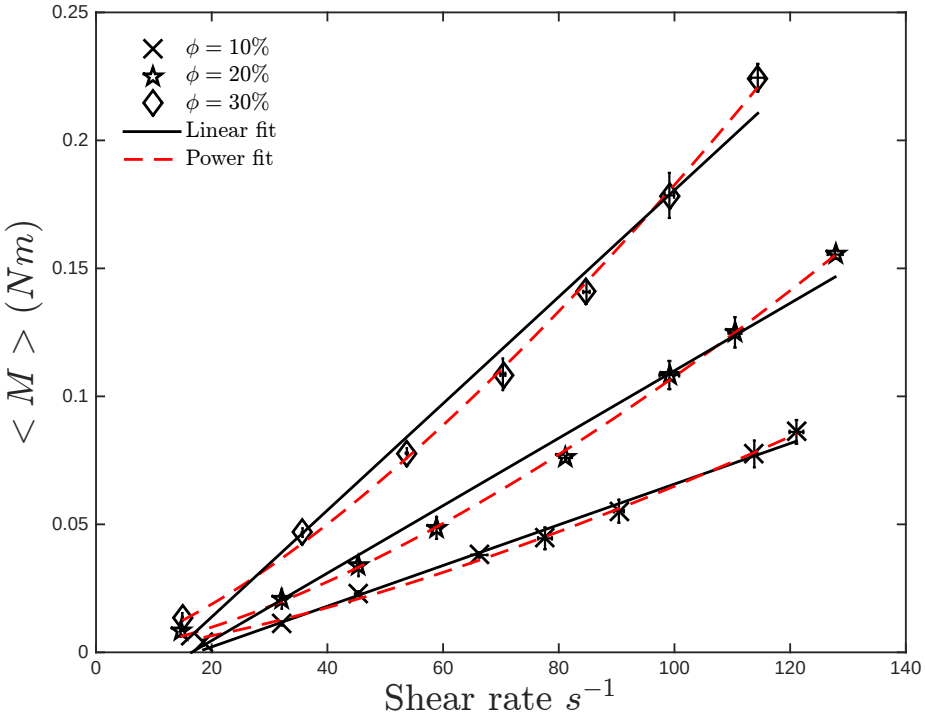

Figure 4.1: Measured torque as a function of shear rate for $\phi = 10$, 20, and 30%. $\rho_p/\rho = 1$. Solid and dashed lines are the linear and power curves fit for the present data. The error bars correspond to the combined uncertainty in the torque measurements.

trend for this set of data is not strictly linear and can also be fitted to a power law, as shown by the dashed lines. The power fit has higher R^2 values than the linear fit ($R^2 = 0.997$ for 10%, $R^2 = 0.999$ for 20% and $R^2 = 0.998$). The exponent of the power fit is around 1.4 for the three volume fractions shown.

Figure 4.2 shows the torque measurements for higher volume fractions of 40% and 50%. Unlike the lower volume fractions, these data are best fitted by a linear fit ($R^2 = 0.997$ for both volume fractions). For these higher volume fractions the intercept of the linear fit is no longer negative. A positive intercept could be a sign of the presence of a yield stress.

The torque measurements were normalized by the theoretical Couette laminar flow torque for the interstitial liquid. Figure 4.3 presents this ratio for the solid fraction of 10, 20, and 30% as a function of Stokes number. If the mixture were strictly Newtonian, this ratio would be equivalent to the relative effective viscosity, and would be independent of the Stokes number (constant viscosity). But as it can be seen in Figure 4.3, the relative viscosity increases with Stokes number. For higher volume fractions the ratio of torques does not appear to vary dramatically with the Stokes number, as shown in Figure 4.4. Only at low Stokes numbers the ratio of $M/M_{laminar}$ for these higher volume fractions exhibits a weak dependance on St, where $M/M_{laminar}$ is greater than that found at higher St.

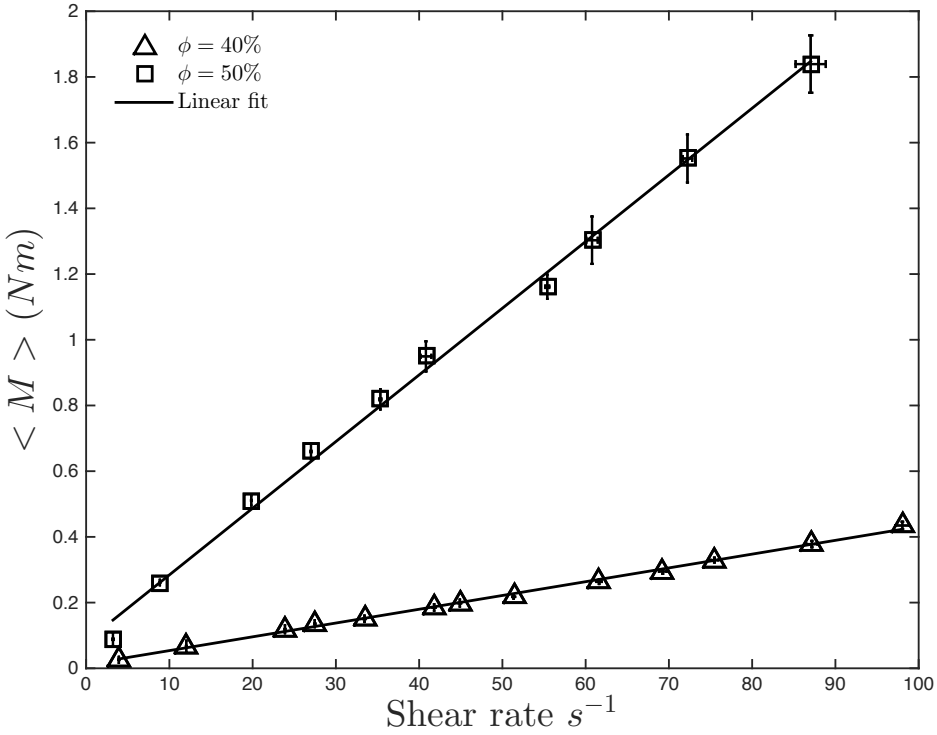

Figure 4.2: Measured torque as a function of shear rate for $\phi = 40$, and 50%. $\rho_p/\rho = 1$. Solid line is the linear curve fit for the present data. The error bars correspond to the combined uncertainty in the torque measurements.

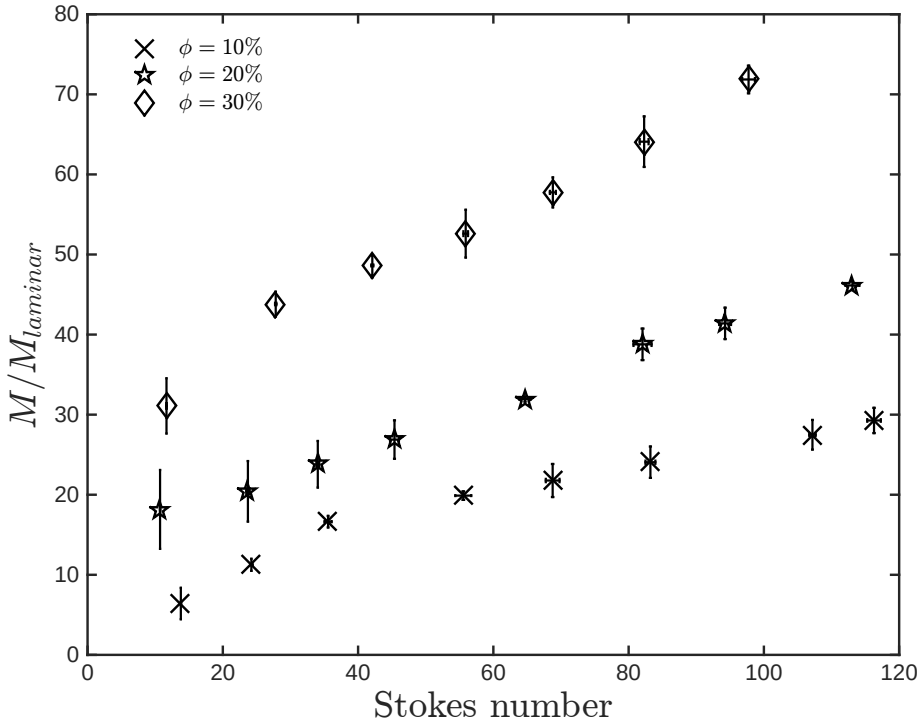

Figure 4.3: Measured torques normalized by the torque predicted from laminar theory as a function of Stokes number for $\phi = 10$, 20, and 30% with $\rho_p/\rho = 1$. The error bars correspond to the combined uncertainty in the torque measurements normalized by the corresponding $M_{laminar}$

The torques ratio exhibits a strong dependance on the volume fraction, varying approximately two orders of magnitude between the lowest and highest volume fraction, as can be observed in Figure 4.5.

In the previous work of Koos (2009) and Koos et al. (2012) it is assumed that the liquid-solid flow is Newtonian, and therefore the ratio of torques, $M/M_{laminar}$, is equal to the relative effective viscosity (μ'/μ). Figure 4.6 shows this ratio μ'/μ for all the Stokes number tested as a function of the volume fraction. The size of the symbols represents the magnitude of the corresponding Stokes number. Note that for volume fractions of 10, 20, and 30%, the ratio of toques exhibits a dependance on Stokes number (equivalently on Reynolds number), where μ'/μ increases with St. The numerical simulations of Yeo and Maxey (2013), Kulkarni and Morris (2008), and Picano et al. (2013) showed also an increase on μ'/μ with Re.

In the previous work of Koos et al. (2012), the relative viscosity for particles with $\rho_p/\rho = 1$ was shown to be an exponential function of the volume fraction normalized with the corresponding particles random loose packing (ϕ_l):

$$\frac{\mu'}{\mu} = exp\Big(8.73\frac{\phi}{\phi_l}\Big).$$

Figure 4.7 shows the relative viscosity as a function of the volume fraction for the present and

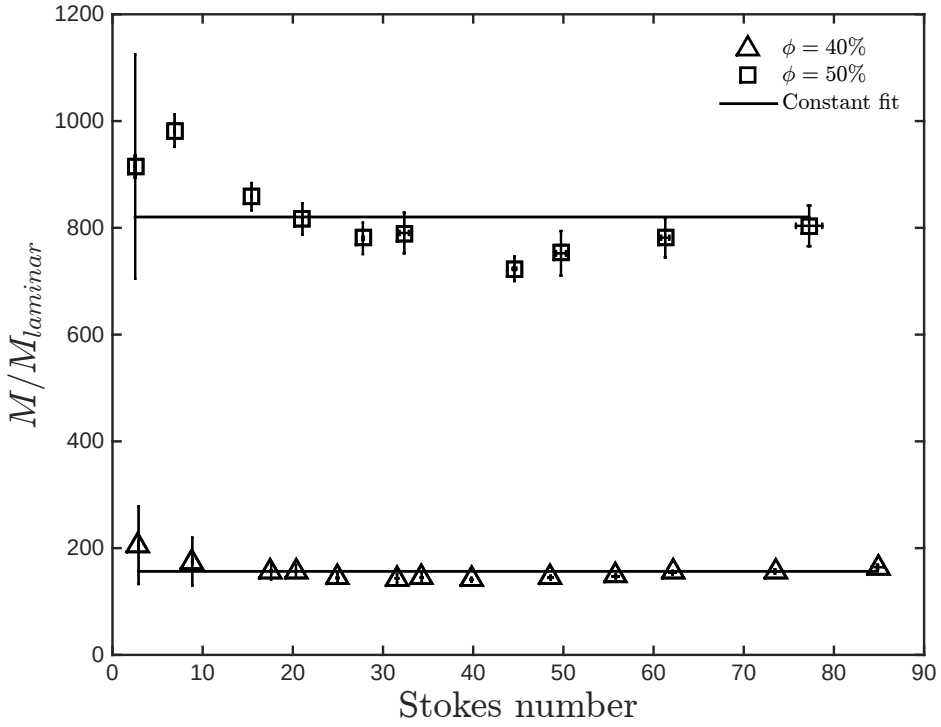

Figure 4.4: Measured torques normalized by the torque predicted from laminar theory as a function of Stokes number for $\phi = 40$ and 50% with $\rho_p/\rho = 1$. Solid lines represent the constant fit for the present data. The error bars correspond to the combined uncertainty in the torque measurements normalized by the corresponding $M_{laminar}$.

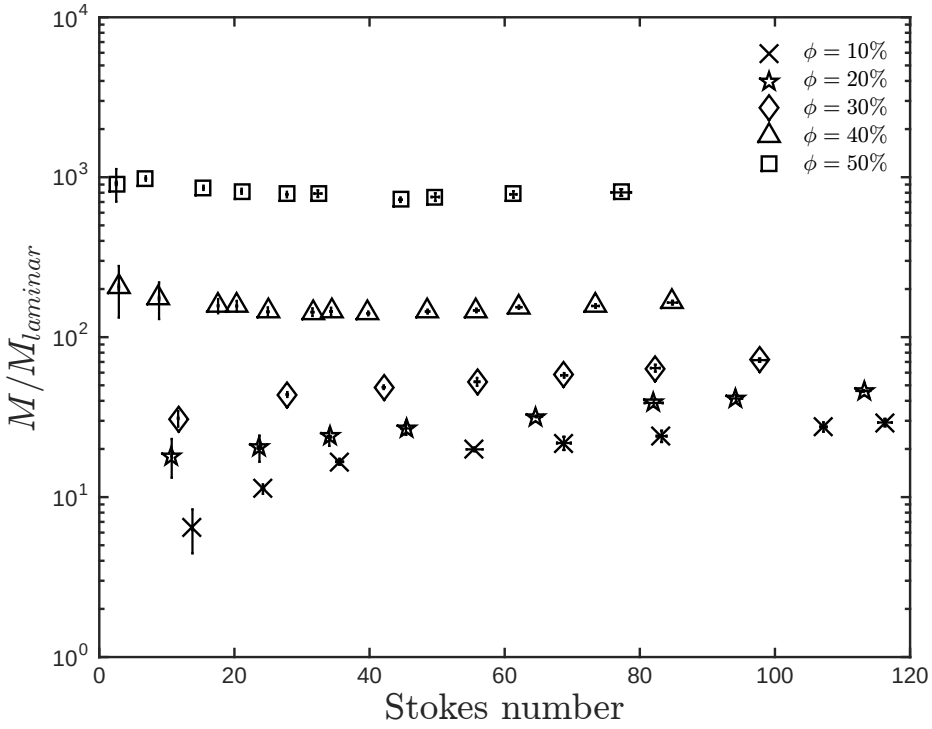

Figure 4.5: Measured torques normalized by the torque predicted from laminar theory as a function of Stokes number for all ϕ tested with $\rho_p/\rho = 1$. The error bars correspond to the combined uncertainty in the torque measurements normalized by the corresponding $M_{laminar}$.

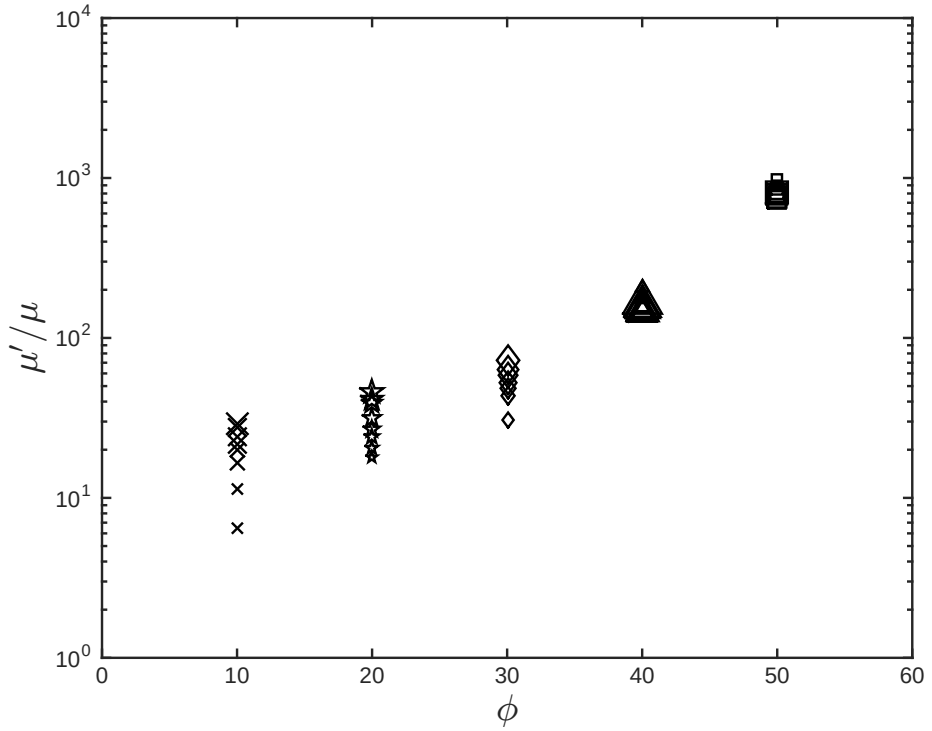

Figure 4.6: Effective relative viscosity as a function of ϕ for experiments with $\rho_p/\rho = 1$. The symbol's size denote the magnitude of the corresponding Stokes number.

previous experiments (Koos, 2009; Koos et al., 2012).

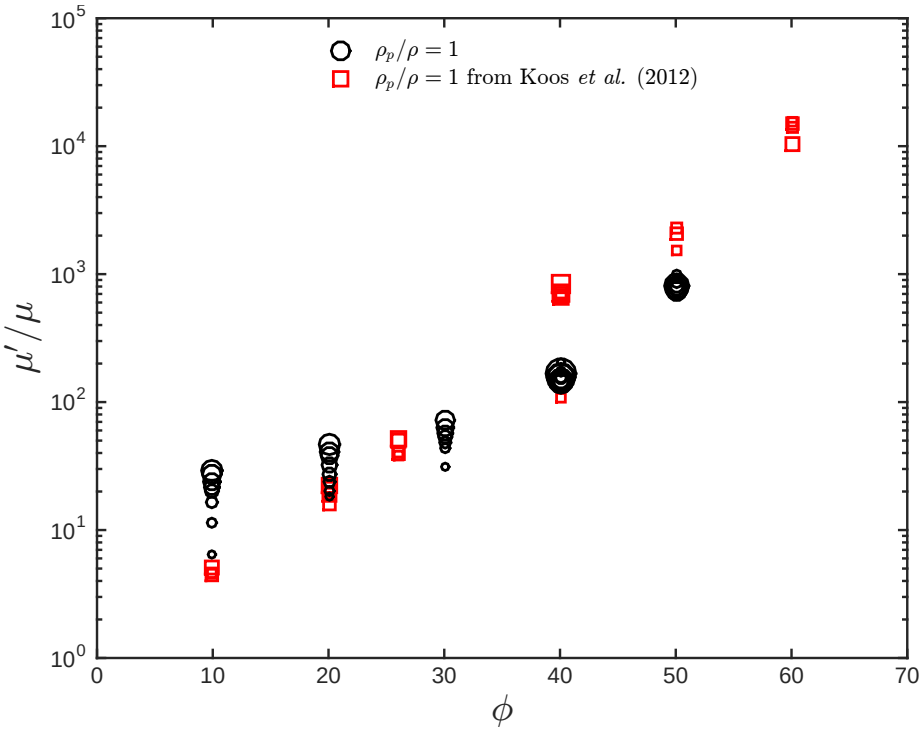

Figure 4.7: Effective relative viscosity as a function of ϕ for the current and previous experiments from Koos et al. (2012) with $\rho_p/\rho = 1$. The symbol's size denote the magnitude of the corresponding Stokes number.

The current and the previous experiments seem to agree in regards to low Stokes numbers. The Stokes numbers tested by Koos et al. (2012) are between 3 and 90, while the current experiments are slightly higher (from 2 to 116). The dependance on Stokes is higher for the current experiments for volume fractions lower than 30%.

4.3 Polystyrene particles with $\rho_p/\rho = 1.05$

To increase the Stokes number tested, experiments with polystyrene particles in water were performed. These particles are denser than water ($\rho_p/\rho = 1.05$) and settle when not sheared. Because the torque measurements are made in the middle section of the rheometer, the effective volume fraction for these experiments may differ from the overall volume fraction. That is, the particles may not be evenly distributed along the rheometer annulus height due to the liquid-solid density mismatch. For instance, at a low volume fraction of 10%, the particles settle at the bottom of the rheometer under static conditions and do not reach the middle section where the torque measurements are taken. Under shearing conditions, the particles fluidize with increasing shear rate, which leads to a presence of a gradient in the particle concentration that depends on the shear rate (an analysis of

the particle fluidization is presented in Chapter 6). For such reason the term loading fraction ($\bar{\phi}$) is used instead of volume fraction. This term denotes the ratio of volume of particles to the total rheometer annulus volume.

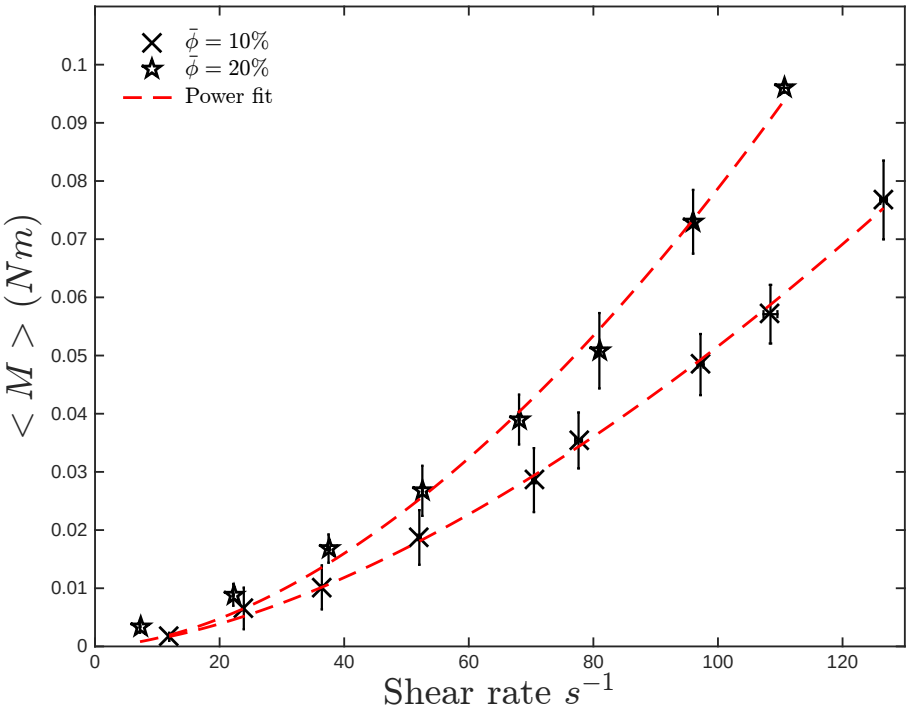

Figure 4.8: Measured torques as a function of shear rate for $\bar{\phi} = 10$ and 20% with $\rho_p/\rho = 1.05$. The dashed lines correspond to the power curve fit for the present data. The error bars correspond to the combined uncertainty in the torque measurements.

Figure 4.8 shows the torque measurements for loading fractions of 10 and 20%. The torque is best fitted by a power law. The fit exponent increases with loading fraction (1.6 for 10% and 1.7 for 20%). This dependance does not hold for higher loading fractions as it can be observed in Figure 4.9 for $\bar{\phi} = 30\%$. In this case the torque is best fitted by a polynomial of order 2. As the loading fraction increases the torque dependance on shear rate varies from a polynomial of order 2 to a polynomial of order 3, as shown in Figure 4.10 and 4.11 for $\bar{\phi} = 40\%$ and $\bar{\phi} = 50\%$.

For a loading fraction of 60% the torque is best fitted by a power law with an exponent smaller than one.

Figure 4.13 shows the results for all the loading fractions tested together with their corresponding curve fit.

Figure 4.14 shows the normalized torque results for loading fractions of 10% and 20% where the increase of $M/M_{laminar}$ with Stokes number can be observed. As the loading fraction increases, the ratio of torques exhibits an opposite behavior: instead of increasing the normalized torques decrease with St as shown in Figure 4.15. The maximum normalized torque for each loading fraction

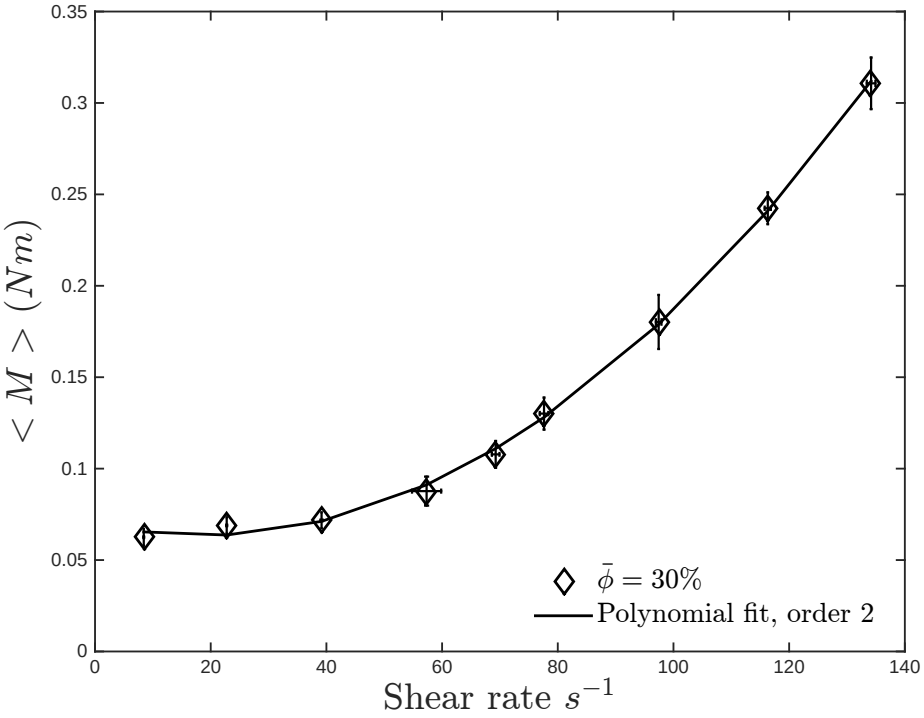

Figure 4.9: Measured torques as a function of shear rate for $\bar{\phi} = 30\%$ with $\rho_p/\rho = 1.05$. The dashed lines correspond to the polynomial curve fit of order 2 for the present data. The error bars correspond to the combined uncertainty in the torque measurements.

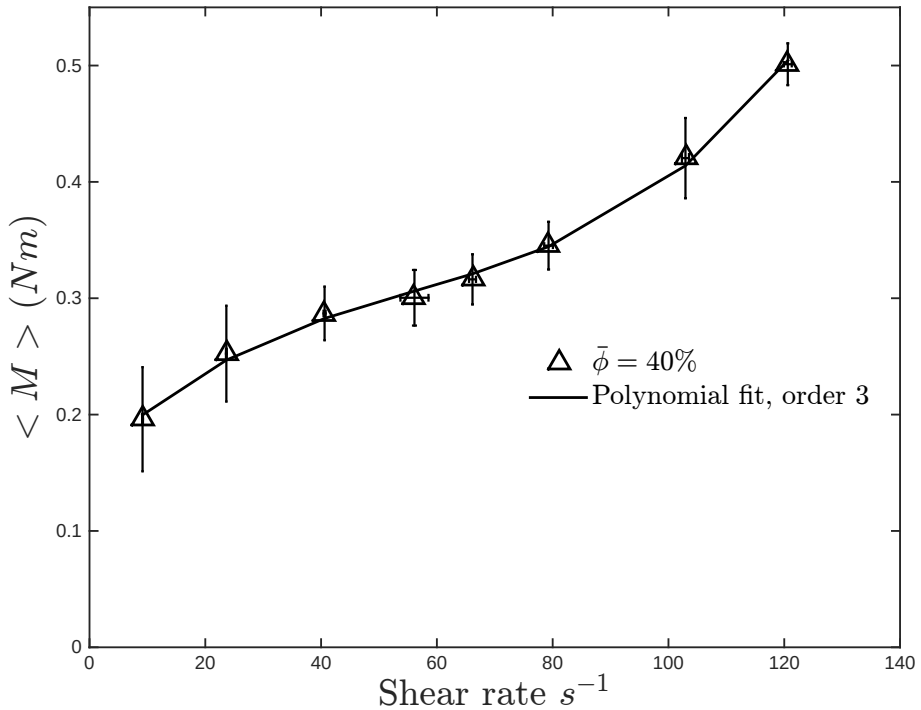

Figure 4.10: Measured torques as a function of shear rate for $\bar{\phi} = 40\%$ with $\rho_p/\rho = 1.05$. The dashed lines correspond to the polynomial curve fit of order 3 for the present data. The error bars correspond to the combined uncertainty in the torque measurements.

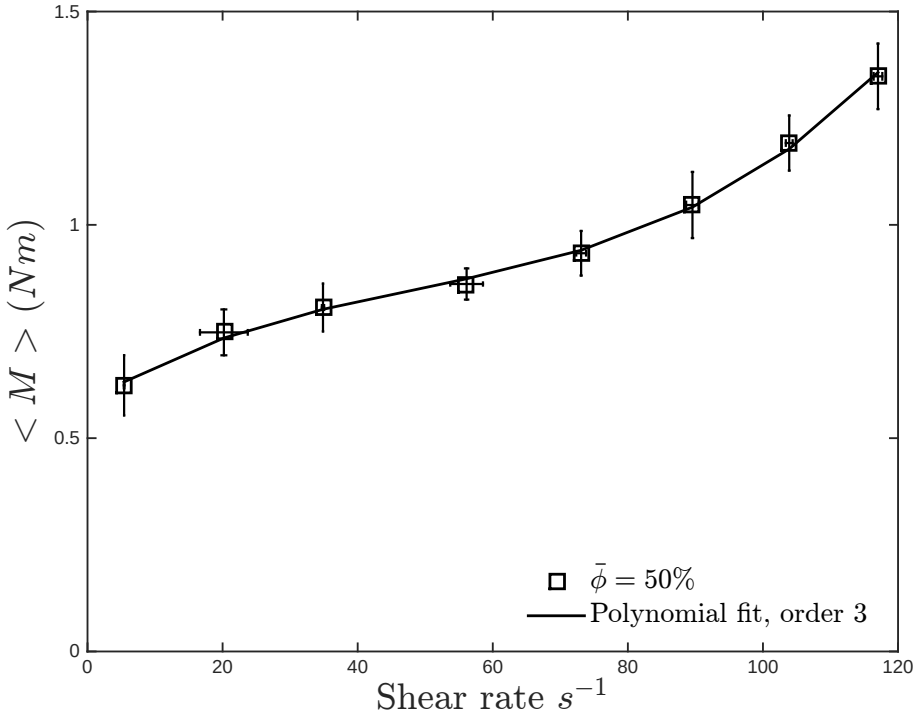

Figure 4.11: Measured torques as a function of shear rate for $\bar{\phi} = 50\%$ with $\rho_p/\rho = 1.05$. The dashed lines correspond to the polynomial curve fit of order 3 for the present data. The error bars correspond to the combined uncertainty in the torque measurements.

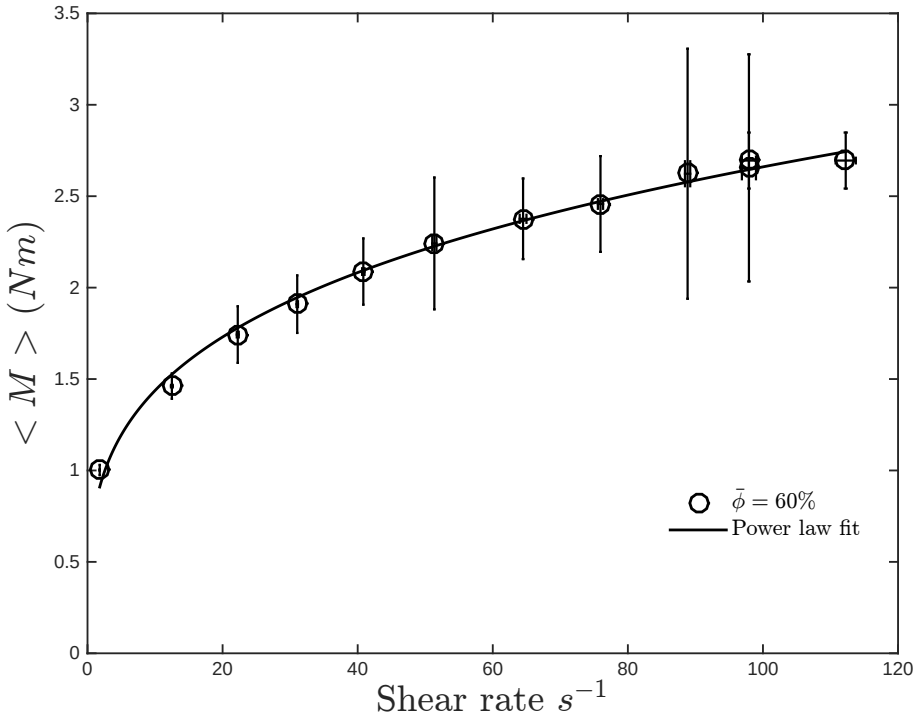

Figure 4.12: Measured torques as a function of shear rate for $\bar{\phi} = 60\%$ with $\rho_p/\rho = 1.05$. The dashed lines correspond to the power curve fit for the present data. The error bars correspond to the combined uncertainty in the torque measurements.

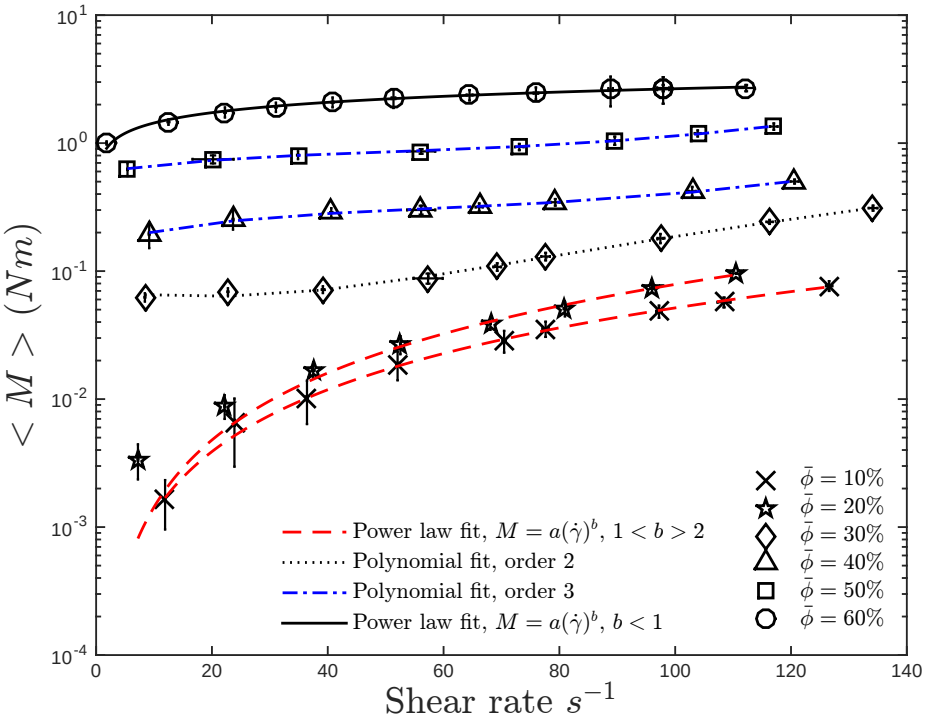

Figure 4.13: Measured torques as a function of shear rate for all $\bar{\phi}$ tested with $\rho_p/\rho = 1.05$. The different lines correspond to the curve fits for the present data. The error bars correspond to the combined uncertainty in the torque measurements.

corresponds to the lowest Stokes number for $\bar{\phi} > 20\%$. For Stokes number above 80, the normalized torques become considerably more independent of the Stokes number. These results are similar to the results found by Acrivos et al. (1994), where the relative effective viscosity of the suspension decreased with increasing shear rate. The apparent shear thinning behavior observed in their work was explained in terms of particle migration due to a slight mismatch on the particle and liquid density. This particle migration led to lower effective volume fractions. A similar mechanism occurs in the present experiments with settling particles. At low shear rates the particles are not fluidized, leading to higher effective volume fractions. A further description of the particle resuspension is given in Chapter 6 and a discussion based on the settling effect is presented in Chapter 7.

As shown in Chapter 6, the measured torques are affected by the fluidization of the particles and the change in effective volume fraction at the test section. A possible explanation for the apparent shear thinning behavior for these loading fraction is the change in effective volume fraction due to the particles resuspension.

Figure 4.16 presents the normalized torques for all the loading fractions tested.

Figure 4.17 shows the relative viscosity as a function of the loading fraction. The size of the symbols denote the magnitude of the Stokes number. For loading fractions of 10 and 20%, the ratio of μ'/μ increases with Stokes numbers. At volume fractions equal to 30% this dependance switches,

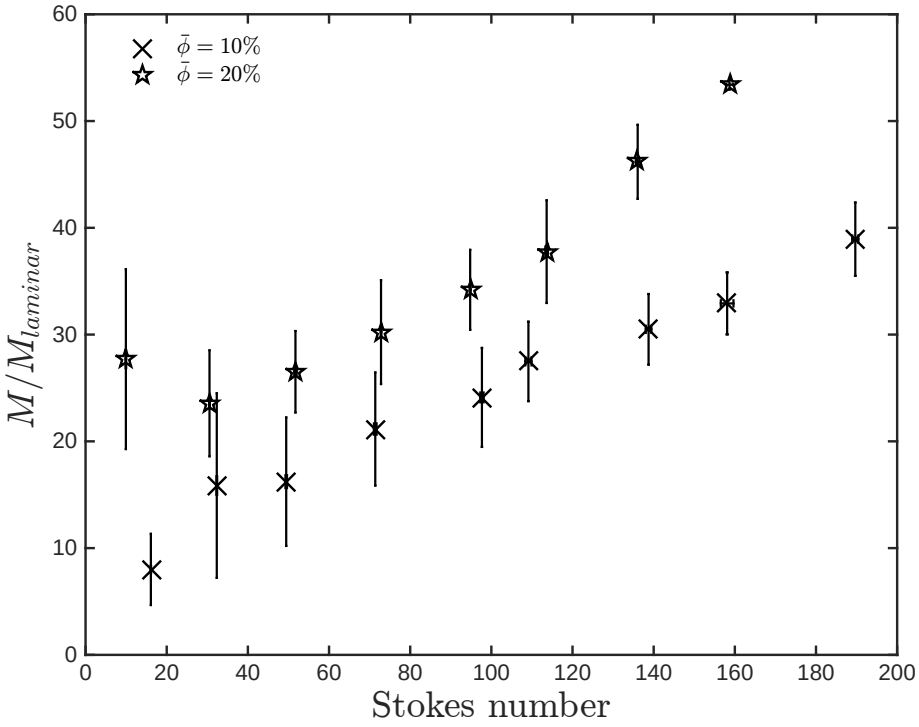

Figure 4.14: Measured torques normalized by the torque predicted from laminar theory as a function of Stokes number for $\bar{\phi} = 10$ and 20% with $\rho_p/\rho = 1.05$. The error bars correspond to the combined uncertainty in the torque measurements normalized by the corresponding $M_{laminar}$.

where the highest ratio of μ'/μ correspond to the lowest Stokes numbers. The change in dependance is discussed in Chapter 7 and it is attributed to the change in effective volume fraction at the test cylinder due to the settling and fluidization of the particles.

4.4 Summary

The results from direct measurements of the torque for $\rho_p/\rho = 1$ and $\rho_p/\rho = 1.05$ are presented. For the case with matched densities, the measured torques exhibit a non-linear dependance on the shear rate for volume fractions below 40%. For $\phi = 40$ and 50%, the dependance of the measured torque on the $\dot{\gamma}$ is linear. The ratio of $M/M_{laminar}$ increases with St for volume fractions of 10, 20, and 30% and become approximately constant for $\phi = 40$ and 50%. At low Stokes number, the $M/M_{laminar}$ for these high volume fractions show some deviation from the constant fit. Comparisons between the current experiments and the previous work of Koos et al. (2012) show that the effective relative viscosity for low Stokes numbers coincides with the previous results (this is assuming that the ratio $M/M_{laminar}$ is equal to μ'/μ). The current results exhibit a higher dependance on the Stokes numbers than the one found by Koos et al. (2012) and for volume fractions higher than 30%, the ratio of μ'/μ is lower than the results of Koos et al. (2012).

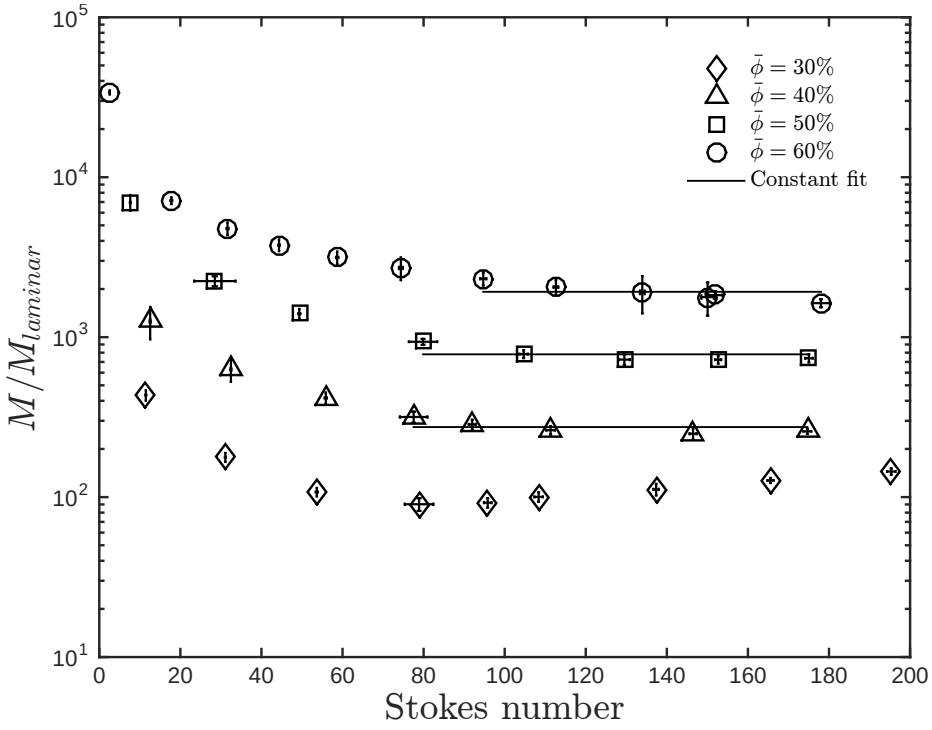

Figure 4.15: Measured torques normalized by the torque predicted from laminar theory as a function of Stokes number for $\bar{\phi} = 10$ and 20% with $\rho_p/\rho = 1.05$. Solid lines correspond to the constant fits for the present data.The error bars correspond to the combined uncertainty in the torque measurements normalized by the corresponding $M_{laminar}$.

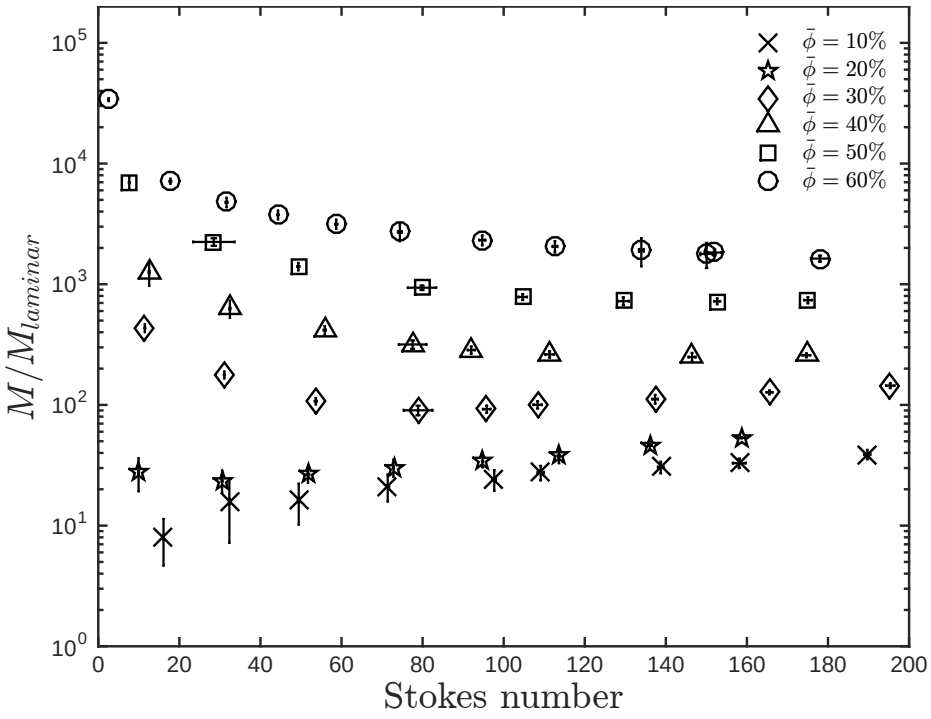

Figure 4.16: Measured torques normalized by the torque predicted from laminar theory as a function of Stokes number for all $\bar{\phi}$ tested with $\rho_p/\rho = 1.05$. The error bars correspond to the combined uncertainty in the torque measurements normalized by the corresponding $M_{laminar}$.

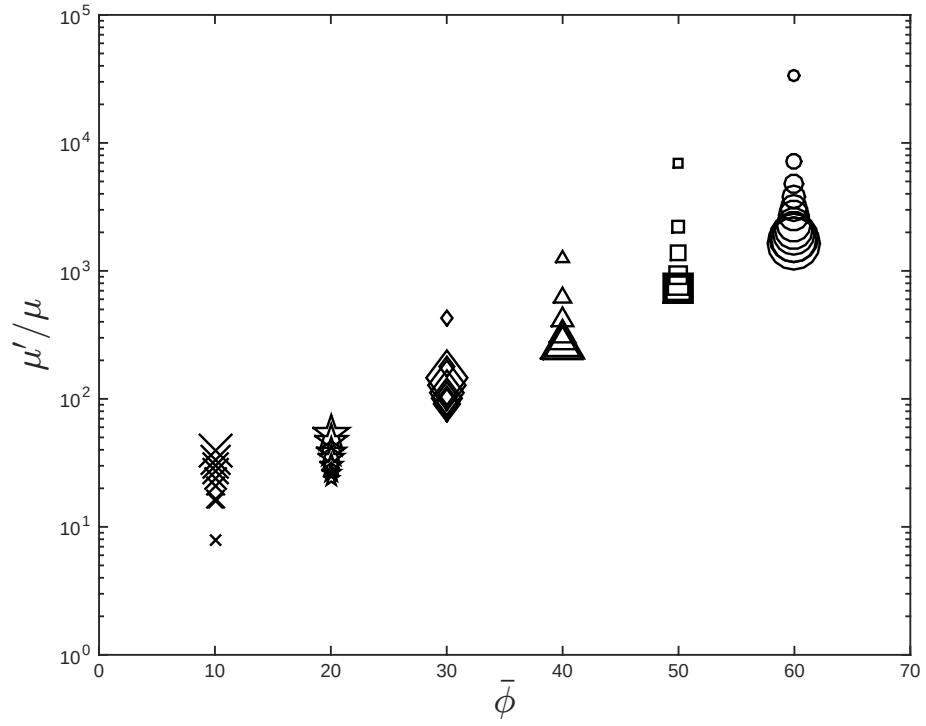

Figure 4.17: Effective relative viscosity as a function of $\bar{\phi}$ for experiments with $\rho_p/\rho = 1.05$. The symbols size denote the magnitude of the corresponding Stokes number.

For the case with settling particles, the measured torques did not show a linear dependance on the shear rate for any of the volume fractions tested. Similarly to the case with matched density, the ratio of torques for loading fractions of 10 and 20% increases with $\dot{\gamma}$ but for higher $\bar{\phi}$, the normalized torques decreases with shear rates. For the particular case of $\bar{\phi} = 30\%$, the ratio of torques decreases with St, and above Stokes number of 80 it starts increasing. For higher volume fractions the normalized torques reaches a plateau above St=80. When plotting the normalized torques as a function of volume fraction a change in Stokes dependance is observed, where for $\bar{\phi} < 30\%$ the ratio of $M/M_{laminar}$ increases with St and for $\bar{\phi} < 30\%$ the dependance is reversed.

Findings from different numerical simulations that considered Reynolds numbers equal or higher than one predict a dependance of the effective relative viscosity with Re (Yeo and Maxey, 2013; Kulkarni and Morris, 2008; Picano et al., 2013). The normalized torques for the case with matched densities and volume fractions lower than 40 exhibit the same trend. However, the Stokes and Reynolds numbers tested in this work are considerably larger than the ones considered in these simulations.

For the case with settling particles the decrease on effective relative viscosity with Stokes numbers for $\bar{\phi} > 20\%$ is similar to the one observed by Acrivos et al. (1994) where particle migration due to a mismatch in densities decreased the effective volume fraction. The same mechanism is presented in this work and it is further analyzed in Chapter 6 and 7.